



Article

A Winter-to-Summer Transition of Bacterial and Archaeal Communities in Arctic Sea Ice

Stefan Thiele^{1,2,*}, Julia E. Storesund³, Mar Fernández-Méndez^{4,5}, Philipp Assmy⁴ and Lise Øvreås^{1,2,6} ¹ Department of Biological Science, University of Bergen, Thormøhlensgate 53 A/B, 5020 Bergen, Norway² Bjerknes Centre for Climate Research, Jahnebakken 5, 5007 Bergen, Norway³ Institute of Marine Research, Nordnesgaten 50, 5005 Bergen, Norway⁴ Norwegian Polar Institute, Fram Centre, Hjalmar Johansens Gate 14, 9296 Tromsø, Norway⁵ Biological Oceanography, GEOMAR Helmholtz Centre of Ocean Research, Düsternbrooker Weg 20, 24105 Kiel, Germany⁶ Department of Arctic Biology, University Center in Svalbard, UNIS, 9171 Longyearbyen, Norway

* Correspondence: stefan.thiele@uib.no

Abstract: The Arctic is warming 2–3 times faster than the global average, leading to a decrease in Arctic sea ice extent, thickness, and associated changes in sea ice structure. These changes impact sea ice habitat properties and the ice-associated ecosystems. Sea-ice algal blooms provide various algal-derived carbon sources for the bacterial and archaeal communities within the sea ice. Here, we detail the transition of these communities from winter through spring to early summer during the Norwegian young sea ICE (N-ICE2015) expedition. The winter community was dominated by the archaeon *Candidatus Nitrosopumilus* and bacteria belonging to the *Gammaproteobacteria* (*Colwellia*, *Kangiellaceae*, and *Nitrinocolaceae*), indicating that nitrogen-based metabolisms, particularly ammonia oxidation to nitrite by *Cand. Nitrosopumilus* was prevalent. At the onset of the vernal sea-ice algae bloom, the community shifted to the dominance of *Gammaproteobacteria* (*Kangiellaceae*, *Nitrinocolaceae*) and *Bacteroidia* (*Polaribacter*), while *Cand. Nitrosopumilus* almost disappeared. The bioinformatically predicted carbohydrate-active enzymes increased during spring and summer, indicating that sea-ice algae-derived carbon sources are a strong driver of bacterial and archaeal community succession in Arctic sea ice during the change of seasons. This implies a succession from a nitrogen metabolism-based winter community to an algal-derived carbon metabolism-based spring/ summer community.

Keywords: Arctic sea ice; biodiversity; microbial ecology; arctic microbes; N-ICE2015; *Nitrosopumilus*; sea-ice algal bloom



Citation: Thiele, S.; Storesund, J.E.; Fernández-Méndez, M.; Assmy, P.; Øvreås, L. A Winter-to-Summer Transition of Bacterial and Archaeal Communities in Arctic Sea Ice. *Microorganisms* **2022**, *10*, 1618. <https://doi.org/10.3390/microorganisms10081618>

Academic Editors: Jiří Bárta and Christopher B. Blackwood

Received: 30 June 2022

Accepted: 28 July 2022

Published: 10 August 2022

Publisher's Note: MDPI stays neutral with regard to jurisdictional claims in published maps and institutional affiliations.



Copyright: © 2022 by the authors. Licensee MDPI, Basel, Switzerland. This article is an open access article distributed under the terms and conditions of the Creative Commons Attribution (CC BY) license (<https://creativecommons.org/licenses/by/4.0/>).

1. Introduction

The increase in global average temperature has pronounced effects on the Arctic [1], leading to a decline in sea-ice extent and thickness and to a change in the sea-ice structure in the Arctic Ocean. The change in ice thickness, quality, and decline in extent has potentially dramatic effects on various aspects of the Arctic ecosystem [2–4]. In 2015, the Norwegian young sea ICE (N-ICE2015) expedition investigated the Arctic sea ice during five and a half months, spanning from Arctic winter to spring and early summer, to investigate the status quo of the atmosphere, the ice, the ocean, and the interconnected ecosystems in the Arctic [5].

During the N-ICE expedition, a pelagic phytoplankton bloom was observed under the ice from late May to late June [6]. This bloom was dominated by the haptophyte *Phaeocystis pouchetii* [6]. The bacterial and archaeal community composition in the water column was investigated, covering the transition from winter to early summer, including the phytoplankton bloom [7]. The bacterial community consisted mainly of *Alpha*- and *Gammaproteobacteria* and changed from a dominance of *Candidatus Pelagibacter* during winter to the dominance of *Gammaproteobacteria* in spring and early summer [7]. This change

in community composition can be attributed to increased carbon source availability derived from the phytoplankton bloom, as such changes have been monitored previously [7,8]. The most prominent difference to temperate waters was found in the high abundance of *Candidatus Nitrosopumilus*, a member of the *Nitrososphaeria* (formerly classified as both Marine Group I *Crenarchaeota* and Marine Group I *Thaumarchaeota*), in the surface samples in winter and a near absence in the summer samples. This decrease is most likely due to photo-inhibition of members of this group at high light regimes in spring and summer and competition with phytoplankton for ammonium in the surface ocean [7,9,10].

In addition to the under-ice phytoplankton bloom, the sea-ice algae bloom dominated by *Nitzschia frigida* was found at the bottom of second-year ice (SYI) [11]. Such blooms are, similarly to pelagic blooms, replenishing the carbon reservoir and enriching the sea-ice environment with easily degradable carbon sources. These carbon sources provide nutrients and energy sources for different members of the bacterial and archaeal community [7,8].

Despite the low temperatures and high salinity in the brine channels, bacterial and archaeal communities thrive in these environments, both in Arctic and Antarctic sea ice. The communities are mostly dominated by *Flavobacteriia* and *Gammaproteobacteria*, but also *Alphaproteobacteria*, *Verrucomicrobia*, and *Bacilli* [12–16]. In winter, a high abundance of *Crenarchaea* of the Marine Group I was found in ice and the underlying water, suggesting an abundance of the ammonia-oxidizing *Candidatus Nitrosopumilus*, which have been classified in this group previously [17,18]. This would suggest more chemolithotrophic metabolisms in winter. In spring and summer metabolisms based on algal-derived carbon sources seem likely. Bacterial and archaeal communities, particularly members of the *Gammaproteobacteria* (especially *Glaciecola* and *Colwellia*) and *Flavobacteriia* (especially *Polaribacter*), have been found in high abundance in connection to phytoplankton blooms in marine environments and similar blooms of sea-ice algae, e.g., *Fragilariopsis cylindrus*, *Nitzschia frigida*, or *Melosira arctica*, which occur in the bottom layers of sea ice in spring/summer [7,8,18–20]. Generally, *Bacteroidia* and *Gammaproteobacteria* have been found in high abundance in Arctic sea ice and brine samples [16,21,22]. However, most samples were analyzed at a higher taxonomic resolution; samples were taken during the summer month and not in winter, and at different geographic locations, including mostly coastal environments [16,21,22]. This might significantly alter the sea-ice bacterial and archaeal communities.

The transition of bacterial and archaeal communities in sea ice from winter to summer is widely unknown. Such studies could elaborate on the status of algal-fueled microbial ecosystems and potentially enable conclusions about the changes in these ecosystems regarding the ongoing effects of global warming. Here, we present a seasonal investigation of microbes in Arctic sea ice from winter to spring and early summer of 2015, hypothesizing an algal-derived carbon sources triggered the succession of the bacterial and archaeal communities.

2. Materials and Methods

2.1. Ice Core Sampling

Ice cores were sampled during the Norwegian young sea ICE (N-ICE2015) expedition from 15 January to 22 June 2015 in the Arctic sea ice pack north of Svalbard, Norway, on board *RV Lance* [5]. During the drift, in total, 7 ice cores were taken from SYI on Floes 1–3 and FYI on Floe 4: 29 January (Floe 1; 83.063° N, 17.582° E), 5 March (Floe 2; 83.142° N, 24.1277° E), 12 March (Floe 2; 82.9296° N; 21.4409° E), 22 April (Floe 3; 82.8478° N, 16.5763° E), 21 May (Floe 3; 81.2328° N, 9.6369° E), 4 June (Floe 3; 80.2939° N, 4.0200° E), and 17 June (Floe 4; 80.4759° N, 7.8683° E; Figure 1). All samples from 29 January to 22 April (Floes 1, 2, and 3) were classified as winter samples, the sample from 21 May (Floe 3) was classified as spring sample, and the samples on 4 and 17 June (Floe 3 and 4) as early summer samples [23]. Due to the necessary changes of Floes, the displayed data do not represent a true time series sampled from a single ice Floe but rather four different ice Floes. The samples were taken using a 14 cm Mark II coring

system (KOVACS enterprise, Roseburg, OR, USA). The bottom 0–10 cm of the core were cut, transferred into a sterile plastic bag, and stored at $-20\text{ }^{\circ}\text{C}$ until further processing. The core parts were thawed for 18–24 h in the dark at $4\text{ }^{\circ}\text{C}$, resulting in $\sim 1.2\text{--}1.3\text{ L}$ of water. Even though this may lead to a shift in the community due to the long melting time, this is not a major issue since bacterial and archaeal growth at this temperature is very low and should not enable fast community changes. In addition, an osmotic shock due to the melting cannot be excluded but seems unlikely given the resulting marine community structure. A total of 1.8 mL of water was set aside for flow cytometry (FCM) analyses, and the remaining water was filtered through $0.2\text{ }\mu\text{m}$ pore size Sterivex filters (Merck, Oslo, Norway). The filters were immediately frozen in liquid nitrogen and then stored at $-80\text{ }^{\circ}\text{C}$. Nitrate and Chl *a* data were retrieved from the general dataset by Assmy [24].

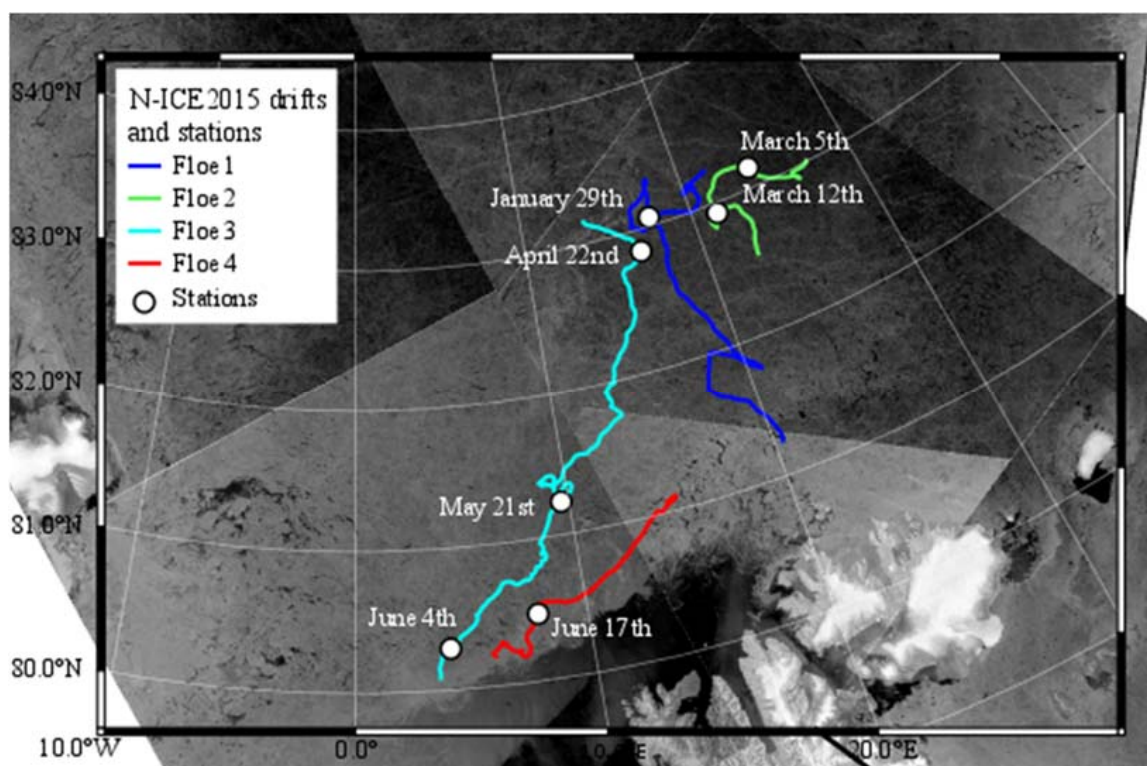


Figure 1. Map of the sampling area with the four different ice Floe drift tracks color-coded and the ice core samples used in/available for this study indicated by date. Image source: RADARSAT-2 image provided by NSC/KSAT under the Norwegian-Canadian RADARSAT agreement. RADARSAT-2 Data and Products[©] MacDonald, Dettwiler and Associates Ltd. (2013) All Rights Reserved. RADARSAT is an official mark of the Canadian Space Agency. Map created by the Norwegian Polar Institute.

2.2. Bacterial Cell Numbers

The triplicates of 1.8 mL FCM samples were fixed with glutaraldehyde (0.5% final conc.) at $4\text{ }^{\circ}\text{C}$ for a minimum of 2 h and then flash frozen in liquid nitrogen and stored at $-80\text{ }^{\circ}\text{C}$ until later analyses. Abundance of bacteria was determined on an Attune Acoustic Flow cytometer (Applied Biosystems by Life technologies, Waltham, MA, USA) with a syringe-based fluidic system using a 20 mW 488 nm blue laser after SYBR-Green staining. Prior to analyses, the samples were thawed and stained with SYBR Green I (Molecular Probes, Eugene, OR, USA) for a minimum of 1 h. Heterotrophic bacteria and archaea were analyzed using a flow rate of $25\text{ }\mu\text{L min}^{-1}$ and HNF at $500\text{ }\mu\text{L min}^{-1}$, following protocols modified from Marie et al. [25].

2.3. DNA and RNA Extraction and Sequencing

For phylogenetic analyses of the bacterial and archaeal diversity and a corresponding inference of their activity, the 16S rRNA genes were sequenced from DNA and RNA extracted from the samples. For that, the Sterivex filters were thawed on ice, and subsequently, a lysis solution was added. DNA and RNA were extracted from filters using the AllPrep DNA/RNA Mini Kit (Qiagen, CA, USA) with a modified protocol as described in Wilson et al. [26]. Briefly, 1 mL extraction buffer was added to each filter, and the filters were vortexed vertically for 2 min, inverted, and vortexed for 2 min. The lysate was removed from the filter and transferred to a 1.5 mL microcentrifuge tube. An AllPrep DNA spin column was loaded with 700 μ L lysate and centrifuged for 30 s at 8000 \times *g*, saving the flow-through for subsequent RNA extraction. Centrifugation steps were repeated for the remaining lysate volume, as necessary. The extracted RNA was treated using the DNA-free DNA Removal kit (Invitrogen, Carlsbad, CA, USA) prior to reverse transcription using the SuperScript III First-Strand Synthesis kit for Real-Time PCR (Invitrogen), according to the manufacturer's instructions. The DNA was quantified using a Qubit 3.0 Fluorometer (Invitrogen, CA, USA). Primer Both cDNA and DNA were then used to prepare sequencing libraries targeting the V4 region of the 16S rRNA genes, using multiplex identifier tagged primers 519F—5'-CAGCMGCCGCGGTAA-3' and 806RB—5'-GGACTACNVGGGTWTCTAAT-3' [27,28]. The 16S rRNA genes were amplified using a two-step nested protocol as described by Wilson et al. [26]. In the first step, PCR amplification was performed in triplicates. The annealing temperature for the PCR reaction was set to 55C and 25 cycles. Multiplex identifier tagged amplicons were pooled in equimolar amounts for library construction. Libraries were sent to the Norwegian Sequencing Center (Oslo, Norway) for sequencing on a MiSeq platform using the MiSeq Reagent Kit v2 (Illumina, San Diego, CA, USA) with paired-end reads of 2 \times 250 bp lengths.

2.4. Sequence Analyses

The retrieved sequences were stored in the European Nucleotide Archive (PRJEB47256) and processed using DADA2 in R [29]. Briefly, primers were removed, and sequences were quality checked based on the illumine quality score before using a quality-based static trim. Amplicon sequence variants (ASVs) were generated from dereplicated reads. After merging the complementary reads and chimera removal, the taxonomy of the ASVs was assigned using a trained Silva database, based on the Silva release SSU Ref NR v138 [30]. ASVs of mitochondria, chloroplasts, and Eukaryotes were removed. An approximate Maximum Likelihood tree was calculated using FastTree2 [31] based on alignments using mafft aligner [32]. NMDS analyses were conducted using weighted Unifrac distances, as well as Constrained Analysis of Principal Coordinates. A Venn diagram for the different seasons was constructed, and Indicator species analyses were employed for the different environmental data. The analyses were done using R 4.1.1. in Rstudio 1.4.1717 and the "vegan 2.5-7", "tidyverse 1.3.1", "phyloseq 1.36.0", "indicspecies 1.7.9", "ggplot2 3.3.5", "RColorBrewer 1.1-2", "forcats 0.5.1", "ggpubr 0.4.0", "patchwork 1.1.1", "scales 1.1.1", "VennDiagram 1.7.0", and "ape 5.5" packages [33–45]. The metabolic potential of the different ASVs was inferred based on their location in a phylogenetic tree of fully sequenced organisms and the genomic assets of the closest relative in this tree using PiCRUST2 2.4.0 with standard parameters in bioconda 0.17.0 [46,47]. Based on enzyme commission (EC) numbers, carbohydrate-active enzymes (CAZymes) belonging to the classes of glycoside hydrolases (GH), polysaccharide lyases (PL), carbohydrate esterases (CE), carbohydrate-binding modules (CBM), and glycosyl transferase (GT), as well as marker genes, namely *nifH*, *nirS/nirK*, *norB*, *nosZ*, *narB*, *napA*, *hzsA*, *amoA-pmoA*, *hao*, *nrfA*, *aprA*, *dsrA*, *cysH*, *soxB*, *mmoX*, *mcrA*, *psaA*, and *psbA*, were used for metabolic analyses (Supplement S1 and S2). CAZymes classified as GH and CBM were only counted as GH.

3. Results

3.1. Cell Numbers and Environmental Data

As reported previously, a sea-ice algae bloom occurred in the bottom part of the ice, with cell numbers of 1.9×10^5 cells mL^{-1} on 21 May and $2.1 \times 10^6 \pm 1.3 \times 10^4$ cells mL^{-1} in June, dominated by the pennate diatom *Nitzschia frigida/neofrigida* [11]. This was confirmed by increasing bulk chlorophyll (Chl) *a* concentration in the lower part of the ice cores from $<0.05 \text{ mg m}^{-3}$ in winter to 6.25 mg m^{-3} in May, 3.15 mg m^{-3} on 4 June, and 1.04 mg m^{-3} on 17 June (Figure 2). Bulk sea-ice nitrate concentrations increased from $0.47 \mu\text{M}$ in January to $1.94 \mu\text{M}$ in April and decreased during spring to $0.92 \mu\text{M}$ on 17 June (Figure 2). The combined bacterial and archaeal cell numbers decreased from 3.5×10^4 cells mL^{-1} in January to 6.4×10^3 cells mL^{-1} on 21 May, before increasing again to 3.0×10^4 cells mL^{-1} and 2.1×10^4 cells mL^{-1} on 4 and 17 June (Figure 2).

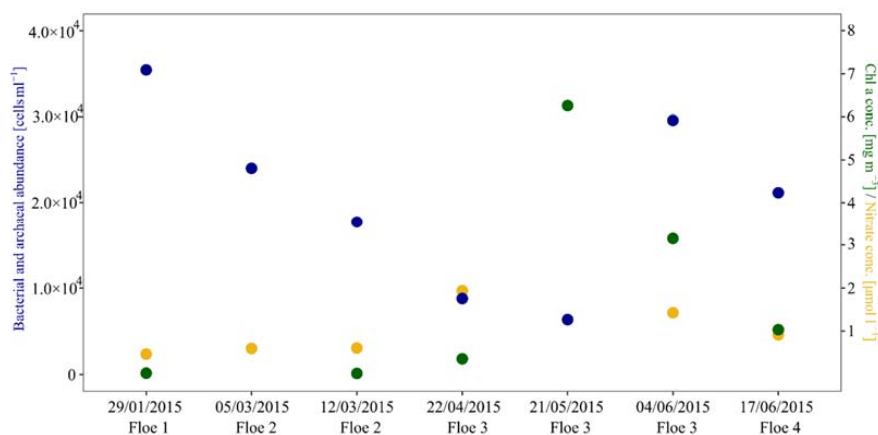


Figure 2. Bacterial and archaeal cell abundance (blue), chlorophyll *a* concentration (green), and nitrate concentration (yellow) during the five months of the N-ICE2015 observation. Gaps in the graph are due to missing values on these days.

3.2. Bacterial and Archaeal Community Composition

The bacterial and archaeal community composition during the N-ICE2015 expedition was investigated using 16S rRNA gene amplicon sequences for community profiling analyses, henceforth shortened to “rel. abundance”, including standard deviations calculated over all samples. This relative abundance was used to calculate the cell abundance in combination with flow-cytometry-derived bacterial and archaeal cell counts.

The most prominent change in the bacterial and archaeal communities is the shift from *Cand. Nitrosopumilus* dominating winter samples to the dominance of *Nitrospiraceae* in spring and *Polaribacter* in early summer. The bacterial community consisted of mainly *Gammaproteobacteria* ($36.9 \pm 6.3\%$ rel. abundance), *Bacteroidia* ($20.6 \pm 12.9\%$ rel. abundance), and *Alphaproteobacteria* ($16.7 \pm 3.2\%$ rel. abundance), complemented with *Verrucomicrobiae* ($3.2 \pm 3.9\%$ rel. abundance), members of the SAR324 clade ($0.9 \pm 0.9\%$ rel. abundance), and several other classes with $<0.5\%$ average rel. abundance (Figure 3). The archaeal community consisted of four classes, with *Nitrososphaeria* ($16.4 \pm 16.1\%$ rel. abundance; Figure 3) being the most abundant and *Halobacteria*, *Nanoarchaeia*, and *Thermoplasmata* being $<0.5\%$ rel. abundance. On this level, a distinct shift from a winter community with high rel. abundance of *Nitrososphaeria* ($27.8 \pm 10.6\%$ rel. abundance) to a spring/early summer community with high rel. abundance of *Bacteroidia* ($33.6 \pm 3.5\%$ rel. abundance) was visible. *Gammaproteobacteria* showed higher rel. abundance in spring/early summer ($41.2 \pm 4.8\%$ rel. abundance) as compared to winter ($33.2 \pm 4.7\%$ rel. abundance), while *Alphaproteobacteria* remained constant in rel. abundance $\sim 18.6\%$ (Figure 3).

The *Nitrososphaeria*, dominated by *Cand. Nitrosopumilus* increased from initial 13.3% rel. abundance in January towards 37.9% of rel. abundance in March and decreased to 0.6% in late June (Figure 3). This is reflected by an increase in cell abundance from 4.7×10^5 cells mL^{-1}

in January to 7.9×10^3 cells mL⁻¹ in March, the highest abundant taxa of the whole dataset, before decreasing to $<3.5 \times 10^2$ cells mL⁻¹ in spring and summer (Figure 4). This dominance of *Cand. Nitrosopumilus* was due to only two ASVs, contributing with 35.1% rel. abundance to the total bacterial and archaeal community on 12 March, thus being the most abundant ASVs in the winter samples.

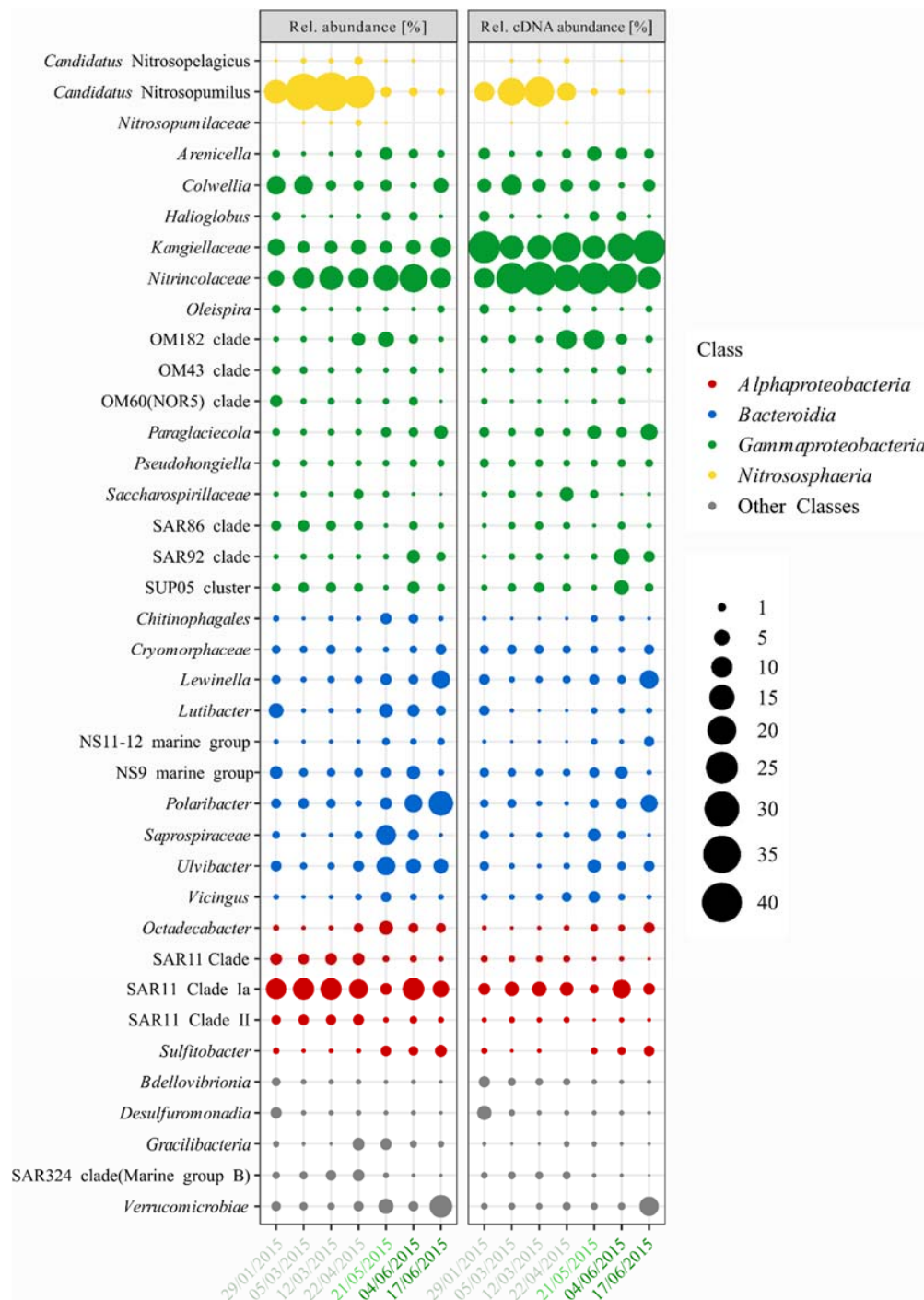


Figure 3. Bubble plot of the most abundant bacterial and archaeal taxa during the N-ICE2015 expedition, which constitute at least 80% of the total community per sample. The plot shows the distribution of 16S rRNA genes (rel. abundance) and RNA the distribution of 16S rRNA copies (rel. cDNA abundance) of the different taxonomic groups. The color of the dates indicates the season (light green = winter, green = spring, and dark green = summer) and the ice algae bloom (dark green).

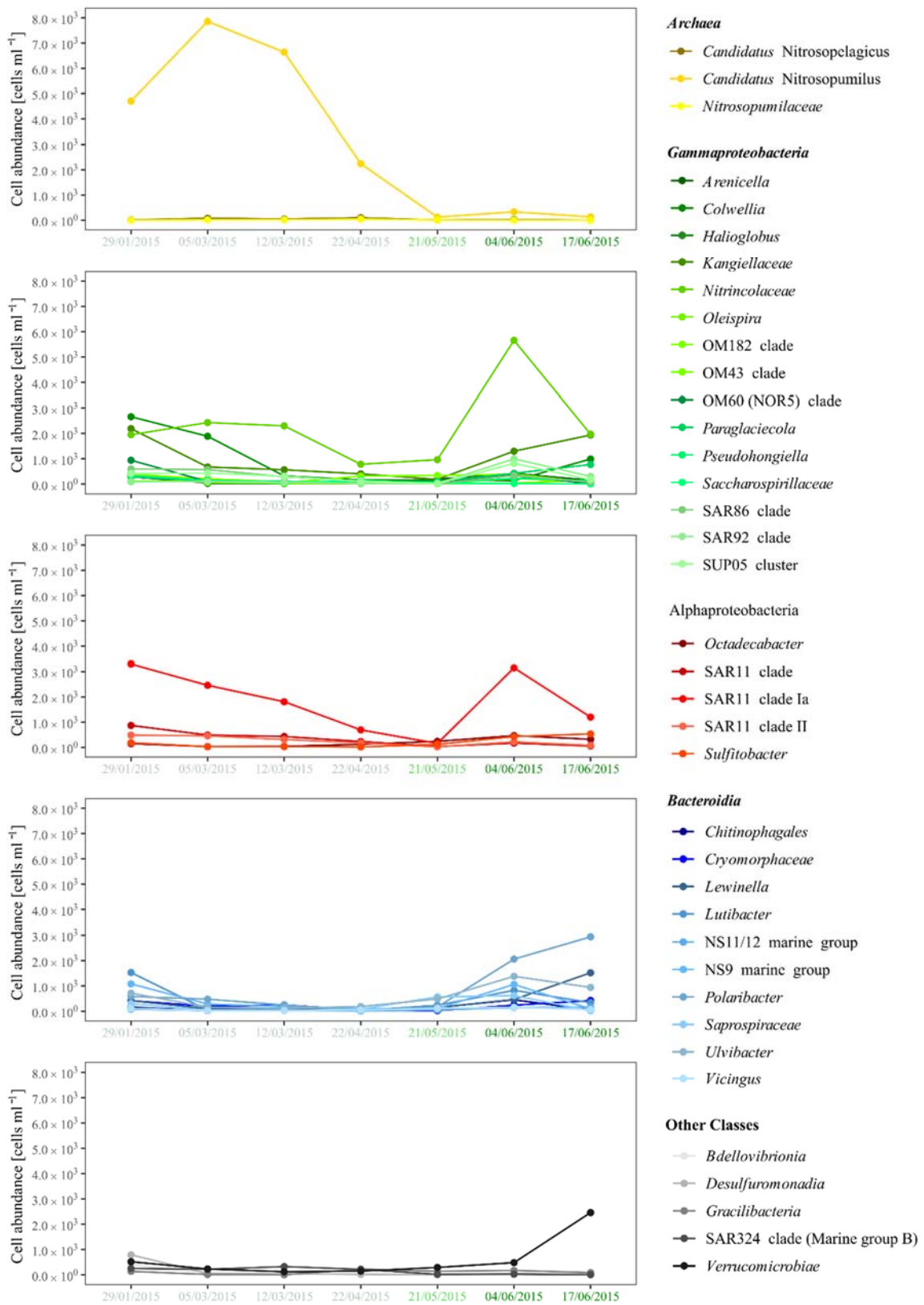


Figure 4. Line plots of bacterial and archaeal abundance of the most abundant taxa based on the rel. abundance and the flow cytometry derived cell numbers. The color of the dates indicates the season (light green = winter, green = spring, and dark green = summer) and the ice algae bloom (dark green).

Bacteroidia decreased from 19.0% in January to 7.3% in March and increased to 35.7% in May, with high rel. abundance of 29.6% on 4 June and 35.5% on 17 June (Figure 3). The high rel. abundance in January was mainly due to *Lutibacter* and members of the NS9 Marine Group (Figure 3), which showed cell abundance of 1.5×10^3 and 1.1×10^3 cells mL⁻¹ (Figure 4). In May, the most dominant groups were *Ulvibacter* and *Saprospiraceae*, followed by *Lutibacter*, *Polaribacter*, *Chitinophagales*, *Lewinella*, *Vicingus*, and members of the NS9 and NS11-12 Marine Groups (Figure 3). During the sea-ice algae bloom *Ulvibacter*, members of the NS9 clade, and *Polaribacter* increased in abundance (Figures 3 and 4). On 17 June, *Polaribacter* increased to 2.9×10^3 cells mL⁻¹, and *Lewinella* increased to 1.5×10^3 cells mL⁻¹, which constituted 13.9% and 7.2% rel. abundance, while *Ulvibacter*, *Lutibacter*, *Saprospiraceae*, and *Chitinophagales* decreased simultaneously (Figures 3 and 4). On the level of ASVs, this succession was dominated by single ASVs for *Lewinella*, *Saprospiraceae*, *Chitinophagales*, *Vicingus*, and members of the NS11-12 Marine Group, while *Lutibacter*, *Polaribacter*, members of the NS9 Marine Group, and *Ulvibacter* were dominated by two ASVs, and only within the *Cryomorphaceae*, six ASVs contributed distinctively to the rel. abundance.

Gammaproteobacteria decreased from 39.2% in January to 28.1% rel. abundance in March and increased to 42.1% in May and to 46.3% on 4 June (Figure 3). Within the *Gammaproteobacteria*, the initially high rel. abundance is based on eleven groups, with *Colwellia*, *Kangiellaceae*, and *Nitrincolaceae* being the most dominant, reaching 2.7×10^3 cells mL⁻¹, 2.2×10^3 cells mL⁻¹, and 2.0×10^3 cells mL⁻¹ (Figures 3 and 4). This was reduced to only five groups in March, where *Nitrincolaceae* was dominant with $11.6 \pm 2.0\%$ rel. abundance (Figure 3), increasing to 2.4×10^3 cells mL⁻¹ and 2.3×10^3 cells mL⁻¹ in this month (Figure 4). The transition from winter to spring was marked mainly by an increase in *Nitrincolaceae* to 19.1% rel. abundance on 4 June and *Kangiellaceae* to 9.2% rel. abundance on 17 June (Figure 3). The peak of *Nitrincolaceae* on 4 June marked the highest cell abundance of a single taxon during the ice algae bloom with 5.7×10^3 cells mL⁻¹ (Figure 4). This succession of *Gammaproteobacteria* was driven mainly by two ASVs assigned to *Nitrincolaceae*, of which one was dominant in winter and May, while the other ASV was abundant in the June samples. Members of the OM43 and OM60 clades, the SUP05 cluster, *Kangiellaceae*, *Arenicella*, and *Paraglaciocola*, were dominated by a single ASVs, while members of the SAR92 and OM182 clades were dominated by two ASVs. Only members of the SAR86 clade with four simultaneously occurring ASVs, and *Colwellia* with one dominant ASV in winter, a second dominant ASV in May, and a third in June showed higher diversity on ASV level.

Alphaproteobacteria were stable at $18.6 \pm 1\%$ rel. abundance throughout the sampling period with decreased rel. abundance of 11.6% and 12.6% on 21 May and 17 June. This was mainly due to a constant abundance of one ASV of the SAR11 clade Ia, which decreased from 3.3×10^3 cells mL⁻¹ in January to 2.6×10^2 cells mL⁻¹ in May, only to increase again to 3.2×10^3 cells mL⁻¹ on 4 June (Figure 4). In contrast, the SAR11 clade II and the SAR11 clade decreased on 21 May and 17 June (Figures 3 and 4). The three main ASVs of *Octadecabacter* increased in rel. abundance on 22 April and 21 May, just to decrease again in summer, while a single ASV of *Sulfitobacter* increased in rel. abundance in May and June (Figure 3); however, the cell abundances of both were constantly below 5.0×10^2 cells mL⁻¹ with the exception of *Sulfitobacter* on 17 June (Figure 4).

Verrucomicrobiae were found with $1.2 \pm 0.5\%$ rel. abundance in the winter samples but increased to 11.6% rel. abundance on 17 June (Figure 3), where they were the second most abundant taxon with 2.5×10^3 cells l⁻¹, second only to *Polaribacter* (Figure 4). This increase was due to a single ASV assigned to *Lentimonas* becoming the most dominant ASV in the community on that day. On the contrary, the members of the SAR324 clade peaked in April, just to decline to <0.1% rel. abundance in June (Figure 3). *Bdellovibrionia* and *Desulfuromonadia* both showed peaks in January with 1.1% and 2.2% rel. abundance.

3.3. Seasonal Variation

Constrained Analysis of Principal Coordinates based on the rel. abundance using the variables with the highest explanatory power (season, ice algae, and days) showed differences between the samples, confirming the differences of the communities between seasons and in correlation to the sea-ice algae bloom (Figure 5). The ice thickness remained fairly constant throughout N-ICE 2015, ranging from 92 cm to 138.5 cm until the floes reached the marginal ice zone, where bottom melting occurred (Supplement S1; [48]).

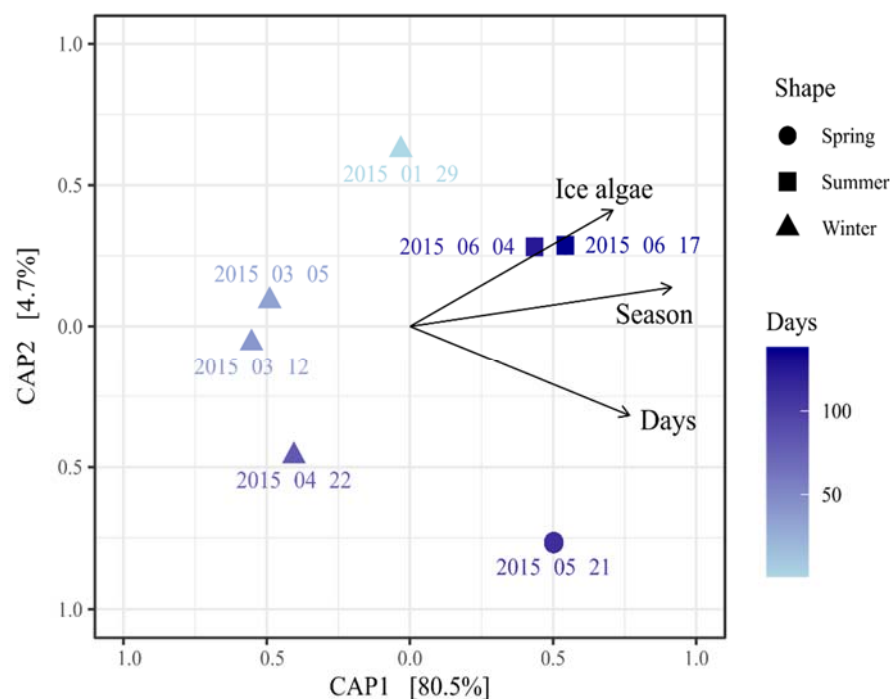


Figure 5. Constrained analysis of principal coordinates analyses including season, ice algae, and days as main factors determining the bacterial and archaeal community.

In winter, 736 ASVs were found (293 unique ASVs), as compared to 173 ASVs (15 unique ASVs) in spring and 351 ASVs (25 unique ASVs) in summer, with 121 ASVs being present in all communities (Figure 6). Using Indicator species analyses, 51 indicative ASVs were found for winter, as compared to eight ASVs for summer. Most of these ASVs were found in low rel. abundance and are thus difficult to interpret given the potential methodological errors and the uncertainties of the importance of low abundance ASVs. However, one ASV of the SAR11 clade was found significantly higher in rel. abundance in winter samples (p -value = 0.012), whereas the main ASV of *Nitriocolaceae* showed significantly higher rel. abundance in summer with $8.2 \pm 0.3\%$ (p -value = 0.012). In addition, one ASV assigned to *Sulfitobacter* was significantly higher in spring and summer with $>1\%$ rel. abundance (p -value = 0.042).

3.4. Bacterial and Archaeal Activity Estimations

Using the relative sequence abundance of 16S rRNA copies as a proxy, the activity of the bacterial and archaeal community was estimated and is stated as “rel. cDNA abundance”. Overall, the rel. cDNA abundance and the rel. abundance are congruent with the most abundant taxa also being the most active (Figure 3). The major finding is the decrease in rel. cDNA abundance of *Cand. Nitrosopumilus* from winter to spring, when the overall active *Kangiellaceae* and *Nitriocolaceae* dominated, and early summer, when *Polaribacter*, *Lewinella*, and *Lentimonas* were most active. The overall activity of the bacterial community was dominated by *Gammaproteobacteria* ($63.3 \pm 7.0\%$ rel. cDNA abundance), *Bacteroidia* ($12.0 \pm 6.8\%$ rel. cDNA abundance), and *Alphaproteobacteria*

($8.9 \pm 2.5\%$ rel. cDNA abundance), complemented by *Verrucomicrobiae* ($1.7 \pm 2.8\%$ rel. cDNA abundance), *Nitrospina* ($1.2 \pm 1.2\%$ rel. cDNA abundance), *Desulfuromonadia* ($0.8 \pm 1.5\%$ rel. cDNA abundance), *Dehalococcoida* ($0.7 \pm 0.8\%$ rel. cDNA abundance), *Bdellovibrionia* ($0.7 \pm 0.7\%$ rel. cDNA abundance), and members of the SAR324 clade ($0.5 \pm 0.4\%$ rel. cDNA abundance; Figure 3). Within the Archaea *Nitrososphaeria* the rel. cDNA abundance of the dominant *Cand. Nitrosopumilus* increased from 8.7% in January to $19.6 \pm 2.5\%$ in March and decreased to $<0.1\%$ during spring and early summer (Figure 3).

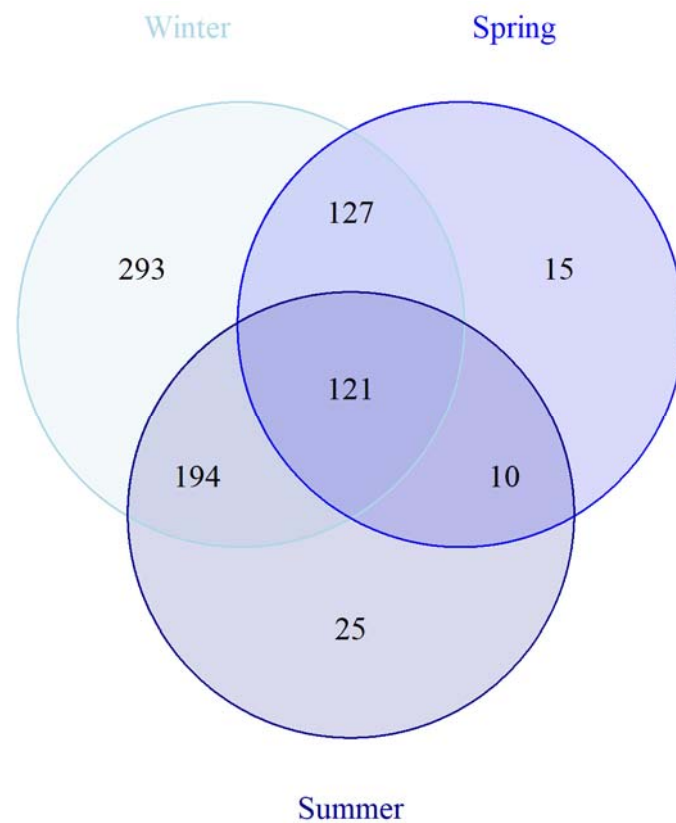


Figure 6. Venn diagram comparing the abundance of the different ASVs for each season (winter = light blue, spring = blue, and summer = dark blue). Each circle represents a season with the number of ASVs specific for the season stated inside. Overlapping areas show the occurrence of specific ASVs in two or all three seasons.

Bacteroidia decreased from 13.3% rel. cDNA abundance in January to $5.8 \pm 0.9\%$ during March and April and increased to 19.1% in May. On 4 June, the rel. cDNA abundance was decreased again to 12.2% before finally increasing to 22.4% on 17 June. The activity patterns in winter showed a high similarity to the abundance patterns of *Polaribacter*, members of the NS9 clade, *Lutibacter*, *Ulvibacter*, *Lewinella*, *Cryomorphaceae*, and *Saprospiraceae* (Figure 3). During the sea-ice algae bloom, *Lewinella*, *Polaribacter*, *Cryomorphyceae*, and members of the NS11-12 Marine Group increased in rel. cDNA abundance on 17 June, while *Vicingus* and *Saprospiraceae* decreased to $<0.5\%$ rel. cDNA abundance (Figure 3).

Gammaproteobacteria rel. cDNA abundance was stable in winter with $59.7 \pm 4.8\%$ and peaked at 73.3% and 71.2% rel. cDNA abundance in May and on 4 June (Figure 3). *Kangiellaceae* and *Nitrincolaceae* were dominant in rel. cDNA abundance throughout the dataset, complemented by *Paraglaciocola*, *Colwellia*, *Arenicella*, *Candidatus Endobugula*, *Saccharospirillaceae*, and members of the OM182, SAR92 clades, and the SUP05 cluster. In winter, the rel. cDNA abundance of *Kangiellaceae* decreased from January to March, while the rel. cDNA abundance of *Nitrincolaceae* increased simultaneously (Figure 3). In the spring and early summer, the rel. cDNA abundance of *Nitrincolaceae* decreased to 11.7% on 17 June, while *Kangiellaceae* increased to 26.7% (Figure 3). *Colwellia* peaked in rel. cDNA

abundance on 5 March, while the members of the OM182 clade peaked in April and May (Figure 3). The rel. cDNA abundance of members of the SUPt05 cluster was highest on 12 March and 4 June, *Arenicella* was highest in May, similar to *Candidatus Endobugula*, while members of the SAR92 were highest on 4 June, and *Paraglaciecola* peaked on 21 May and 17 June, showing a succession among the *Gammaproteobacteria* (Figure 3).

The rel. cDNA abundance of *Alphaproteobacteria* was stable with $9.1 \pm 0.1\%$ in winter, increased to 13.3% in spring/ early, and decreased again to 8.1% on 17 June (Figure 3). SAR11 Clade Ia peaked in rel. cDNA abundance on 4 June (Figure 3). *Sulfitobacter* and *Octadecabacter* were low in winter but increased in rel. cDNA abundance on 17 June (Figure 3).

The rel. cDNA abundance of *Verrucomicrobiae* was stable at $0.7 \pm 0.2\%$ but increased on 17 June to 8.1% due to an increase in *Lentimonas* rel. cDNA abundance (Figure 3). Members of the SAR324 clade showed a rel. cDNA abundance <1% (Figure 3). Congruent with the peaks in rel. abundance in January, *Bdellovibrionia* and *Desulfuromonadia* showed peaks in rel. cDNA abundance of 2.2% and 4.1% (Figure 3).

3.5. Functional Approximation Based on PiCRUST2

The metabolic potential of the different ASVs inferred using PiCRUST2 bears problems in the form of representativeness of the inferred genome. This is especially true at ASV level and in underrepresented environments, which are both not covered well in the databases. Therefore, even the genomes determined as closest to the ASV might still differ to some extent from the true genome of the ASV [49]. Therefore, the results of these analyses have to be treated carefully and represent only an estimation, not measured metagenomes. The predictions using PiCRUST2 resulted in 827 “metagenomes” with weighted Nearest Sequenced Taxon Index values < 1.0. NSTI indicates the phylogenetic distance to the nearest neighbor in the genome database. Among the CAZymes, all classes besides PLs were found with >0.2% rel. abundance and showed an increase from winter to spring and early summer (Figure 7). GHs increased significantly ($p = 0.011$; t -test) from $0.41 \pm 0.11\%$ to 0.95% in spring and $0.80 \pm 0.18\%$ in early summer (Figure 7). GTs were stable at $0.61 \pm 0.03\%$ rel. abundance, while CE and CBM increased significantly ($p = 0.006$ and 0.023 ; t -test) from $0.17 \pm 0.03\%$ and $0.23 \pm 0.03\%$ to 0.29% and 0.34% in spring and $0.24 \pm 0.01\%$ and $0.31 \pm 0.05\%$ in early summer (Figure 7). The distribution of CAZymes was relatively even among the *Gammaproteobacteria*, with GH and PL mostly found in *Glaciecola*, *Paraglaciecola*, and *Colwellia*; CE in *Cellvibrionaceae*; and CBM and GT in *Colwellia*, UBA10353 Marine Group, and *Pseudomonas*. In addition, members of the SAR86 and OM182 clades showed a high abundance of GT. Within the *Bacteroidia*, GH, CE, CBM, and GT distribution was dominated by *Saprospiraceae*, *Cryomorphaceae*, and members of the NS9 Marine Group, while PL were found almost exclusively in *Polaribacter*. *Alphaproteobacteria* possessed mainly GT and some CBM, dominated by members of the SAR11 Clade II and *Magnetospiraceae*. The CE found in *Verrucomicrobiae* were mainly predicted for *Roseibacillus* and *Rubritalea*.

Among the marker genes, only *nirS/nirK* (Denitrification), *amoA* (Nitrification), *aprA* (Dissimilatory sulphate reduction), and *cysH* (Assimilatory sulfate reduction) reached a rel. abundance of >0.05%, while *nifH* (Nitrogen fixation), *norB* (Denitrification), *nosZ* (Denitrification), *narB* (Assimilatory nitrate reduction), *hao* (Nitrification), *nrfA* (Dissimilatory nitrate reduction to ammonium), and *dsrA* (Dissimilatory sulfite reduction) were predicted in low abundance (<0.01%), and *hzsA* (Annamox), *soxB* (Sulphur oxidation), *mmoX* (Aerobic methane oxidation), *mcrA* (Methanogenesis), *psaA* (Photosynthesis), and *psbA* (Photosynthesis) were not predicted (Figure 7). Since the *amoA* and *pmoA* genes are very similar and the genes were almost exclusively predicted for *Cand. Nitrosopumilus*, known to possess *amoA* [50], the predictions were considered as *amoA*. The *amoA*, as well as *nirS/nirK* were most abundant in winter samples with $0.10 \pm 0.05\%$ and $0.05 \pm 0.02\%$, rel. abundance and decreased significantly (both $p = 0.011$) to <0.01% in spring and early summer (Figure 7). The abundance of *amoA* was clearly dominated by *Cand. Nitrosopumilus*, but also predicted for *Gammaproteobacteria* (Figure 7). Within the *Bacteroidia*, *nirS/nirK* and *norB* were predicted for *Aurantivirga*, *Flavobacterium*, and *Tenacibaculum*.

Most genes for denitrification predicted for *Gammaproteobacteria* were found in *Colwellia* and *Pseudomonas* (*nirS/nirK* and *nosZ*, Figure 7). For the archaeal *Nitrosphaeria* only the abundance of *nirS/nirK* was predicted, distributed mainly to *Cand. Nitrosopelagicus* and *Nitrosopumilaceae*. The marker gene for assimilatory nitrate reduction (*narB*) was found in *Polaribacter*, *Arcobacteraceae*, and *Synechococcus*, while nitrogen fixation (*nifH*) was predicted for *Bdellovibrionia* (members of the OM27 clade), *Campylobacteria* (*Arcobacteraceae*), and *Desulfuromonadia* (members of the PB19 clade; Figure 7).

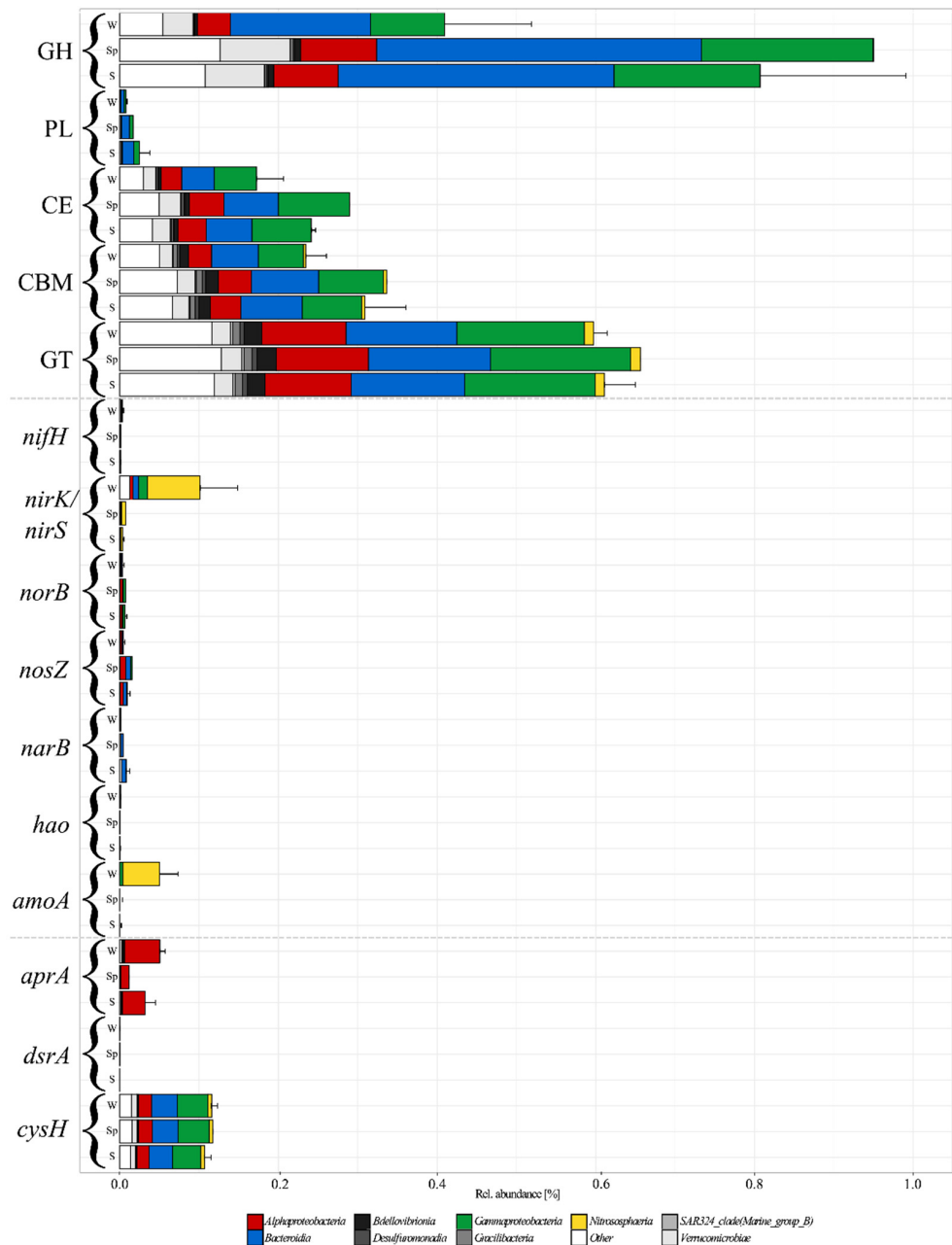


Figure 7. Rel. abundance of predicted CAZyme classes (glycoside hydrolases (GH), polysaccharide lyases (PL), carbohydrate esterases (CE), carbohydrate-binding modules (CBM), and glycosyl transferase (GT) and marker gene abundances for the three distinct seasons (Winter (W), Spring (Sp), and Summer (S)). The rel. abundance is shown as % of total genes detected in the PiCRUST2 inferred metagenome for each sample. The error bars show the variability in the four stations pooled for the winter sample and the two stations for the summer sample. No error bar is available for spring since only one sample was taken in this season. The bars include the predicted taxonomic assignment of the respective CAZyme classes and marker genes on class level.

The *aprA* gene was present in winter with $0.05 \pm 0.01\%$, decreased significantly ($p = 0.032$) to 0.01% in spring and increased again to $0.03 \pm 0.01\%$ in early summer. The marker genes for dissimilatory sulfate reduction and oxidation (*aprA* and *dsrA*) were predicted for members of the OM27 clade (*Bdellovibrionia*), *Desulfofrigus* (*Desulfobacteria*), *Desulforhopalus* (*Desulfobulbia*), and PB19 (*Desulfuromonadia*), and members of the SAR11 clades Ia, II, and further unspecified members, as well as members of the AEGEAN-169 Marine Group only *aprA*. The *cysH* gene was predicted stable at $0.11 \pm 0.01\%$ rel. abundance in all samples and for a large variety of classes, dominated by *Cryomorpaceae* and members of the NS9 Marine Group in the *Bacteroidia*, while *Magnetospiraceae* dominated the abundance in the *Alphaproteobacteria*, members of the OM182 clade the *Gammaproteobacteria*, and *Lentimonas* and *Roseibacillus* the *Verrucomicrobia*.

4. Discussion

Here, we describe the transition of the bacterial and archaeal communities of Arctic sea ice from winter to spring and early summer. Even though this is not a true time series due to the necessary relocation in drifting ice, the samples taken on Floe 3 (April to June) show a clear succession of the bacterial and archaeal community. The community from April matches the communities from January and March (Floes 1 and 2), while the community from 17 June (Floe 4) is similar to 4 June (Floe 3). Thus, suggesting comparability of samples. In addition, the high taxonomic resolution of the ASVs supports the comparability since most ASVs were found in most or all samples.

An ice algal bloom of the pennate diatom *Nitzschia frigida* dominated the bottom ice algal assemblage of both FYI and SYI in May and June. Other pennate diatoms, unidentified flagellates, and resting cells (particularly of the dinoflagellate *Polariella glacialis*) came next in importance, while centric diatoms and ciliates occurred at low abundances (Supplement S1; [11]). *Melosira arctica* occurred at low abundances, and the only records of this species were from slurp gun samples taken by divers below sea-ice ridges. The characteristic mats of this species were not observed. The ice algal bloom corresponds to an increase in light availability in the ice, enabling phototrophic growth. A decrease in nitrate concentrations was only observed around 22 May, when sea-ice algae cell numbers increased more rapidly [11]. A succession of the bacterial and archaeal community based on the algae-derived carbon sources was observed in the bottom layer of the sea ice from winter to early summer.

4.1. The Winter Community

The most drastic change was the vanishing of *Cand. Nitrosopumilus*, from high abundance in winter to near absence in summer, as is congruent with the findings in Arctic surface waters [7,26,51,52]. *Cand. Nitrosopumilus* performs nitrification [17], thus explaining the high rel. abundance of *nirS/nirK* and *amoA* predicted for *Cand. Nitrosopumilus*. This indicates that ammonium oxidation to nitrite could be a key metabolism in winter months and, combined with nitrite oxidation, could lead to the replenishment of the nitrate pool in the sea ice [53]. The nitrite oxidizing *Nitrospina*, often associated with *Cand. Nitrosopumilus* [54–56], was found in low rel. abundance < 1% but high rel. cDNA abundance in winter samples (~3–4% rel. cDNA abundance). However, gammaproteobacterial *Nitrincolaceae* (formerly *Oceanospirillaceae*) may also use nitrite oxidation as the main energy source, thus explaining the relatively high abundance during winter and adding to the production of nitrate [57,58]. Photoinhibition was assumed to be a factor for *Cand. Nitrosopumilus* mortality and would explain the near absence in light conditions in spring and early summer [10,59,60]. In addition, ammonium is the most easily accessible nitrogen source for algae, which leads to competition for ammonium when light is present [9,61]. Even though *Cand. Nitrosopumilus* is adapted to very low ammonia concentrations, the competition could add to the explanation of the decreasing rel. cDNA abundance of *Cand. Nitrosopumilus* in April and the near disappearance of this taxon during the sea-ice algae bloom. However, this would not explain the decreased rel. cDNA abundance in January,

which might correlate to the lower abundance in this sample. In addition, competition with fast-growing members of the *Gammaproteobacteria* and *Bacteroidia* could lead to a decrease in *Cand. Nitrosopumilus* in carbon-replenished spring and summer samples [59,62,63].

Members of the alphaproteobacterial SAR11 clade are resilient, slow-growing organisms with low requirements for carbon sources and high abundance in oligotrophic polar oceans [64–67], thus explaining the indicator function of one ASV of the SAR11 Clade in winter. The abundance of the *aprA* gene in winter samples is due to the abundance of members of SAR11 clades. *AprA/B* has been found in SAR11 previously, and dissimilatory sulfate oxidation has been suspected [68,69]. The higher abundance of genes indicating nitrogen and sulfur metabolisms in winter samples supports the hypothesis of a bacterial and archaeal community, where limited carbon sources lead to shifts towards other, e.g., nitrogen-based metabolisms. In addition, members of the SUP05 cluster, reported in Antarctic surface waters, harbor the genetic requirements for chemolithoautotrophic carbon assimilation using nitrate and reduced sulfur compounds [52,58,70]. Members of the SAR324 clade were found to use lithotrophy, heterotrophy, and alkane oxidation simultaneously [71] and have been found in Arctic surface and under-ice waters [7]. Still, their role in this ecosystem remains unknown. The abundance of sulfur-reducing *Desulfuromonadia* [72] also points toward alternative metabolisms in winter.

4.2. A Carbon-Based Succession in Spring/Early Summer

Gammaproteobacteria and *Bacteroidia* are usually found in eutrophic, carbon-rich marine environments, often in correlation with phytoplankton blooms, thus explaining their abundance in the spring and early summer samples [8,73–79]. The most abundant Gammaproteobacteria in these samples, *Nitrincolaceae*, members of the OM182 and SAR92 clades, and the *Alteromonadaceae* groups *Arenicella*, *Paraglaciecola*, and *Colwellia*, have been found in association with phytoplankton blooms and polar waters [8,80–83]. *Nitrincolaceae* harbor a high diversity of carbon metabolisms, explaining their abundance during the sea-ice algae bloom [83,84]. *Kangiellaceae* were suggested to extracellularly utilize amino acid as carbon and nitrogen sources, explaining the abundance of *Kangiellaceae* in early winter and summer samples [85]. *Bacteroidia* harbor a multitude of carbon degradation pathways, leading to successions of different groups after phytoplankton blooms [8,77,79]. In various marine and sea-ice environments, *Polaribacter* co-occur with phytoplankton blooms [8,19,67,86,87], explaining the high abundance of this group in spring and early summer. High abundances of members of the NS9 clade have also been found in summer and fall in samples from Antarctica and were correlated to phytoplankton appearance in early spring in the Southern Ocean [88,89]. In addition, members of the *Verrucomicrobiae*, specifically *Lentimonas*, degrade complex carbon sources, and hence have been found in later stages of phytoplankton blooms [8,90–92]. *Rhodobacteraceae*, such as *Sulfitobacter* and *Octadecabacter*, are often correlated to diatom blooms [8,83,93]. Thus, a sea-ice algae-derived carbon-source-driven succession of the bacterial and archaeal community in spring and early summer is congruent with the finding of significantly different communities between seasons and with ASVs of *Nitrincolaceae* and *Sulfitobacter* being indicator species for spring and early summer. This succession might even go on after early summer, as samples from Arctic sea ice and brines with a high abundance of different taxa within the *Gammaproteobacteria* and *Bacteroidia* indicate [16,21,22]. One explanation for these differences could be that a further succession throughout summer and fall could lead to increased carbon source production, which then could fuel even the winter community. This may explain the higher abundance of several taxa within the *Gammaproteobacteria* (*Nitrincolaceae*, *Kangiellaceae*, and *Colwellia*) and *Bacteroidia* (*Lewinella*, *Lutibacter*, *Polaribacter*, and members of the NS9 marine group). However, due to the lack of fall samples in this study and the geographical distances between the studies, this has to remain a hypothesis.

4.3. CAZyme Abundance Support Succession Based on Carbon Sources

The pattern of increased predicted CAZyme abundance in Bacteroidia and Gammaproteobacteria in spring and early summer, as compared to winter, is based on the abundance of these taxa. Therefore, an increase in CAZymes indicates the potential of the various genera within the Bacteroidia and Gammaproteobacteria to utilize different carbon sources and, consequently, different ecological niches. These community patterns are also congruent with the finding in a sample from adjacent first-year ice (FYI), where a similar bloom occurred [11], and the pelagic communities in the *P. pouchetii* bloom observed below the ice starting on 25 May [6], where a succession of the bacterial and archaeal community in the surface waters from *Alphaproteobacteria* and *Cand. Nitrosopumilus* in winter to *Gammaproteobacteria* and *Bacteroidia* in spring and early summer was found [7]. This correlation seems to be independent of the bloom-forming species, implying that the variety of carbon sources provided by the bloom-forming algae is broadly similar. This implies that functional guilds in the bacterial and archaeal community are not specialized to a single algal species, even though specific ASVs might be dependent on specific algae species [93]. This could also explain the similarity to the algae-derived carbon-source-based bacterial and archaeal successions found in phytoplankton bloom in the arctic as well as temperate waters [7,8,77].

5. Conclusions

Here, we report the community composition and activity of Arctic sea-ice *Bacteria* and *Archaea* during the transition from winter to early summer in 2015 north of Svalbard. We show the transition of this community from a winter state with decreasing cell numbers, mostly nitrogen-based metabolisms, and dominance of *Cand. Nitrosopumilus* from January to an early spring state in March. There, nitrification potentially replenished the nitrate pool, which could then be used by other organisms during spring and summer. In spring, *Bacteroidia* and *Gammaproteobacteria* increased in abundance, while *Cand. Nitrosopumilus* nearly vanished. The succession of *Gammaproteobacteria* and *Bacteroidia* is driven by season and the corresponding availability of carbon sources derived from the light-induced, diatom-dominated ice algal spring bloom, which leads to the establishment of different ecological niches, subsequently exploited by the best-adapted groups. Given the changes in arctic environments based on global warming, this seasonal succession from dominantly nitrogen-based to dominantly carbon-based cycling could be interrupted or accelerated by alteration in the sea-ice environment, potentially leading to changes in the microbial sea-ice ecosystem.

Supplementary Materials: The following supporting information can be downloaded at: <https://www.mdpi.com/article/10.3390/microorganisms10081618/s1>. Supplement S1: List of environmental data per station; Supplement S2: DNA sequence counts, rel. abundance, and cell abundance (a); and RNA sequence counts and rel. cDNA abundance (b) per station; Supplement S3: List of CAZymes including the total inferred abundance of the gene per sample; Supplement S4: List of marker genes by metabolism including the total inferred abundance of the gene per sample.

Author Contributions: Conceptualization, P.A. and L.Ø.; Methodology, S.T., J.E.S., M.F.-M., P.A. and L.Ø.; Investigation, S.T.; Writing—Original Draft Preparation, S.T.; Writing—Review and Editing, J.E.S., M.F.-M., P.A. and L.Ø.; Supervision, L.Ø. and P.A.; Project Administration, P.A.; Funding Acquisition, P.A. All authors have read and agreed to the published version of the manuscript.

Funding: The N-ICE2015 expedition was funded by the former Centre for Ice, Climate, and Ecosystems (ICE) at the Norwegian Polar Institute. This work was funded by the ERANet LAC project number ELAC2014/DCC-0178 and the Research Council of Norway through the CAVEICE (number 256162) and Boom or Bust (number 244646) projects.

Data Availability Statement: All sequences are stored in the European Nucleotide Archive (PRJEB47256).

Acknowledgments: We would like to acknowledge the captain and crew of the *RV Lance*. Furthermore, we thank Hanna M. Kauko, Lasse M. Olsen and Mats A. Granskog for additional data, the map in Figure 1, and discussions.

Conflicts of Interest: The authors declare no conflict of interest.

References

1. Meier, W.N.; Hovelsrud, G.K.; van Oort, B.E.H.; Key, J.R.; Kovacs, K.M.; Michel, C.; Haas, C.; Granskog, M.A.; Gerland, S.; Perovich, D.K.; et al. Arctic Sea Ice in Transformation: A Review of Recent Observed Changes and Impacts on Biology and Human Activity. *Rev. Geophys.* **2014**, *52*, 185–217. [[CrossRef](#)]
2. Maslanik, J.; Stroeve, J.; Fowler, C.; Emery, W. Distribution and Trends in Arctic Sea Ice Age through Spring 2011. *Geophys. Res. Lett.* **2011**, *38*, L13502. [[CrossRef](#)]
3. Lindsay, R.; Schweiger, A. Arctic Sea Ice Thickness Loss Determined Using Subsurface, Aircraft, and Satellite Observations. *Cryosphere* **2015**, *9*, 269–283. [[CrossRef](#)]
4. Kwok, R. Arctic Sea Ice Thickness, Volume, and Multiyear Ice Coverage: Losses and Coupled Variability (1958–2018). *Environ. Res. Lett.* **2018**, *13*, 105005. [[CrossRef](#)]
5. Granskog, M.A.; Fer, I.; Rinke, A.; Steen, H. Atmosphere-Ice-Ocean-Ecosystem Processes in a Thinner Arctic Sea Ice Regime: The Norwegian Young Sea ICE (N-ICE2015) Expedition. *J. Geophys. Res. Oceans* **2018**, *123*, 1586–1594. [[CrossRef](#)]
6. Assmy, P.; Fernández-Méndez, M.; Duarte, P.; Meyer, A.; Randelhoff, A.; Mundy, C.J.; Olsen, L.M.; Kauko, H.M.; Bailey, A.; Chierici, M.; et al. Leads in Arctic Pack Ice Enable Early Phytoplankton Blooms below Snow-Covered Sea Ice. *Sci. Rep.* **2017**, *7*, 40850. [[CrossRef](#)]
7. De Sousa, A.G.G.; Tomasino, M.P.; Duarte, P.; Fernández-Méndez, M.; Assmy, P.; Ribeiro, H.; Surkont, J.; Leite, R.B.; Pereira-Leal, J.B.; Torgo, L.; et al. Diversity and Composition of Pelagic Prokaryotic and Protist Communities in a Thin Arctic Sea-Ice Regime. *Microb. Ecol.* **2019**, *78*, 388–408. [[CrossRef](#)]
8. Teeling, H.; Fuchs, B.M.; Bennke, C.M.; Krüger, K.; Chafee, M.; Kappelmann, L.; Reintjes, G.; Waldmann, J.; Quast, C.; Glöckner, F.O.; et al. Recurring Patterns in Bacterioplankton Dynamics during Coastal Spring Algae Blooms. *eLife* **2016**, *5*, e11888. [[CrossRef](#)]
9. Christman, G.D.; Cottrell, M.T.; Popp, B.N.; Gier, E.; Kirchman, D.L. Abundance, Diversity, and Activity of Ammonia-Oxidizing Prokaryotes in the Coastal Arctic Ocean in Summer and Winter. *Appl. Environ. Microbiol.* **2011**, *77*, 2026–2034. [[CrossRef](#)]
10. Merbt, S.N.; Stahl, D.A.; Casamayor, E.O.; Martí, E.; Nicol, G.W.; Prosser, J.I. Differential Photoinhibition of Bacterial and Archaeal Ammonia Oxidation. *FEMS Microbiol. Lett.* **2012**, *327*, 41–46. [[CrossRef](#)]
11. Olsen, L.M.; Laney, S.R.; Duarte, P.; Kauko, H.M.; Fernández-Méndez, M.; Mundy, C.J.; Rösel, A.; Meyer, A.; Itkin, P.; Cohen, L.; et al. The Seeding of Ice Algal Blooms in Arctic Pack Ice: The Multiyear Ice Seed Repository Hypothesis. *J. Geophys. Res. Biogeosci.* **2017**, *122*, 1529–1548. [[CrossRef](#)]
12. Brinkmeyer, R.; Knittel, K.; Jürgens, J.; Weyland, H.; Amann, R.; Helmke, E. Diversity and Structure of Bacterial Communities in Arctic versus Antarctic Pack Ice. *Appl. Environ. Microbiol.* **2003**, *69*, 6610–6619. [[CrossRef](#)]
13. Bowman, J.S.; Rasmussen, S.; Blom, N.; Deming, J.W.; Rysgaard, S.; Sicheritz-Ponten, T. Microbial Community Structure of Arctic Multiyear Sea Ice and Surface Seawater by 454 Sequencing of the 16S RNA Gene. *ISME J.* **2012**, *6*, 11–20. [[CrossRef](#)]
14. Cowie, R.O.M.; Williams, G.J.; Maas, E.W.; Voyles, K.M.; Ryan, K.G. Antarctic Sea-Ice Microbial Communities Show Distinct Patterns of Zonation in Response to Algal-Derived Substrates. *Aquat. Microb. Ecol.* **2014**, *73*, 123–134. [[CrossRef](#)]
15. Han, D.; Kang, I.; Ha, H.K.; Kim, H.C.; Kim, O.-S.; Lee, B.Y.; Cho, J.-C.; Hur, H.-G.; Lee, Y.K. Bacterial Communities of Surface Mixed Layer in the Pacific Sector of the Western Arctic Ocean during Sea-Ice Melting. *PLoS ONE* **2014**, *9*, e86887. [[CrossRef](#)] [[PubMed](#)]
16. Boetius, A.; Anesio, A.M.; Deming, J.W.; Mikucki, J.A.; Rapp, J.Z. Microbial Ecology of the Cryosphere: Sea Ice and Glacial Habitats. *Nat. Rev. Micro.* **2015**, *13*, 677–690. [[CrossRef](#)]
17. Könneke, M.; Bernhard, A.E.; de la Torre, J.R.; Walker, C.B.; Waterbury, J.B.; Stahl, D.A. Isolation of an Autotrophic Ammonia-Oxidizing Marine Archaeon. *Nature* **2005**, *437*, 543–546. [[CrossRef](#)]
18. Collins, R.E.; Rocap, G.; Deming, J.W. Persistence of Bacterial and Archaeal Communities in Sea Ice through an Arctic Winter. *Environ. Microbiol.* **2010**, *12*, 1828–1841. [[CrossRef](#)]
19. Eronen-Rasimus, E.; Piiparinen, J.; Karkman, A.; Lyra, C.; Gerland, S.; Kaartokallio, H. Bacterial Communities in Arctic First-Year Drift Ice during the Winter/Spring Transition. *Environ. Microbiol. Rep.* **2016**, *8*, 527–535. [[CrossRef](#)]
20. Eronen-Rasimus, E.; Luhtanen, A.-M.; Rintala, J.-M.; Delille, B.; Dieckmann, G.; Karkman, A.; Tison, J.-L. An Active Bacterial Community Linked to High Chl-*a* Concentrations in Antarctic Winter-Pack Ice and Evidence for the Development of an Anaerobic Sea-Ice Bacterial Community. *ISME J.* **2017**, *11*, 2345–2355. [[CrossRef](#)]
21. Fernández-Gómez, B.; Díez, B.; Polz, M.F.; Arroyo, J.I.; Alfaro, F.D.; Marchandon, G.; Sanhueza, C.; Farías, L.; Trefault, N.; Marquet, P.A.; et al. Bacterial Community Structure in a Sympagic Habitat Expanding with Global Warming: Brackish Ice Brine at 85–90 °N. *ISME J.* **2019**, *13*, 316–333. [[CrossRef](#)] [[PubMed](#)]

22. Torstensson, A.; Margolin, A.R.; Showalter, G.M.; Smith, W.O., Jr.; Shadwick, E.H.; Carpenter, S.D.; Bolinesi, F.; Deming, J.W. Sea-Ice Microbial Communities in the Central Arctic Ocean: Limited Responses to Short-Term PCO₂ Perturbations. *Limnol. Oceanogr.* **2021**, *66*, S383–S400. [[CrossRef](#)]
23. Cohen, L.; Hudson, S.R.; Walden, V.P.; Graham, R.M.; Granskog, M.A. Meteorological Conditions in a Thinner Arctic Sea Ice Regime from Winter to Summer during the Norwegian Young Sea Ice Expedition (N-ICE2015). *J. Geophys. Res. Atmos.* **2017**, *122*, 7235–7259. [[CrossRef](#)]
24. Assmy, P.; Dodd, P.A.; Duarte, P.; Dujardin, J.; Elliott, A.; Fernández-Méndez, M.; Fransson, A.; Granskog, M.A.; Hendry, K.; Hodgson, R.; et al. *N-ICE2015 Sea Ice Biogeochemistry*; Norwegian Polar Institute: Tromsø, Norway, 2017. [[CrossRef](#)]
25. Marie, D.; Brussaard, C.P.D.; Thyrhaug, R.; Bratbak, G.; Vaultot, D. Enumeration of Marine Viruses in Culture and Natural Samples by Flow Cytometry. *Appl. Environ. Microbiol.* **1999**, *65*, 45–52. [[CrossRef](#)]
26. Wilson, B.; Müller, O.; Nordmann, E.-L.; Seuthe, L.; Bratbak, G.; Øvreås, L. Changes in Marine Prokaryote Composition with Season and Depth Over an Arctic Polar Year. *Front. Mar. Sci.* **2017**, *4*, 95. [[CrossRef](#)]
27. Øvreås, L.; Forney, L.; Daae, F.L.; Torsvik, V. Distribution of Bacterioplankton in Meromictic Lake Saelenvannet, as Determined by Denaturing Gradient Gel Electrophoresis of PCR-Amplified Gene Fragments Coding for 16S rRNA. *Appl. Environ. Microbiol.* **1997**, *63*, 3367–3373. [[CrossRef](#)]
28. Apprill, A.; McNally, S.; Parsons, R.; Weber, L. Minor Revision to V4 Region SSU rRNA 806R Gene Primer Greatly Increases Detection of SAR11 Bacterioplankton. *Aquat. Microb. Ecol.* **2015**, *75*, 129–137. [[CrossRef](#)]
29. Callahan, B.J.; McMurdie, P.J.; Rosen, M.J.; Han, A.W.; Johnson, A.J.A.; Holmes, S.P. DADA2: High-Resolution Sample Inference from Illumina Amplicon Data. *Nat. Meth.* **2016**, *13*, 581–583. [[CrossRef](#)]
30. Quast, C.; Pruesse, E.; Yilmaz, P.; Gerken, J.; Schweer, T.; Yarza, P.; Peplies, J.; Glockner, F.O. The SILVA Ribosomal RNA Gene Database Project: Improved Data Processing and Web-Based Tools. *Nucl. Acids Res.* **2013**, *41*, D590–D596. [[CrossRef](#)]
31. Price, M.N.; Dehal, P.S.; Arkin, A.P. FastTree 2—Approximately Maximum-Likelihood Trees for Large Alignments. *PLoS ONE* **2010**, *5*, e9490. [[CrossRef](#)]
32. Katoh, K.; Misawa, K.; Kuma, K.; Miyata, T. MAFFT: A Novel Method for Rapid Multiple Sequence Alignment Based on Fast Fourier Transform. *Nucl. Acids Res.* **2002**, *30*, 3059–3066. [[CrossRef](#)] [[PubMed](#)]
33. Cáceres, M.D.; Legendre, P. Associations between Species and Groups of Sites: Indices and Statistical Inference. *Ecology* **2009**, *90*, 3566–3574. [[CrossRef](#)] [[PubMed](#)]
34. Chen, H.; Boutros, P.C. VennDiagram: A Package for the Generation of Highly-Customizable Venn and Euler Diagrams in R. *BMC Bioinform.* **2011**, *12*, 35. [[CrossRef](#)] [[PubMed](#)]
35. McMurdie, P.J.; Holmes, S. Phyloseq: An R Package for Reproducible Interactive Analysis and Graphics of Microbiome Census Data. *PLoS ONE* **2013**, *8*, e61217. [[CrossRef](#)] [[PubMed](#)]
36. Neuwirth, E. *RColorBrewer: ColorBrewer Palettes*, R Package Version 1.1-2; 2014. Available online: <https://rdrr.io/cran/RColorBrewer/man/ColorBrewer.html> (accessed on 29 June 2022).
37. Wickham, H. *Ggplot2: Elegant Graphics for Data Analysis*; Springer: New York, NY, USA, 2016.
38. Wickham, H. *Forcats: Tools for Working with Categorical Variables (Factors)*, R Package Version 0.5.0.; 2020. Available online: <https://forcats.tidyverse.org/reference/forcats-package.html> (accessed on 29 June 2022).
39. Paradis, E.; Schliep, K. Ape 5.0: An Environment for Modern Phylogenetics and Evolutionary Analyses in R. *Bioinformatics* **2019**, *35*, 526–528. [[CrossRef](#)]
40. Wickham, H.; Averick, M.; Bryan, J.; Chang, W.; McGowan, L.D.; François, R.; Grolemund, G.; Hayes, A.; Henry, L.; Hester, J.; et al. Welcome to the Tidyverse. *J. Open Source Softw.* **2019**, *4*, 1686. [[CrossRef](#)]
41. Kassambara, A. *Ggpubr: “ggplot2” Based Publication Ready Plots*, R Package Version 0.4.0. 2020. Available online: <https://rpkgs.datanovia.com/ggpubr/> (accessed on 29 June 2022).
42. Lin Pedersen, T. *Patchwork: The Composer of Plots*, R Package Version 1.1.0. 2020. Available online: <https://patchwork.data-imaginist.com/> (accessed on 29 June 2022).
43. Oksanen, J.; Blanchet, F.G.; Friendly, M.; Kindt, R.; Legendre, P.; McGinn, D.; Minchin, P.R.; O’Hara, R.B.; Simpson, G.L.; Solymos, P.; et al. *Vegan: Community Ecology Package*, R Package Version 2.5-7. 2020. Available online: <https://github.com/vegandevs/vegan> (accessed on 29 June 2022).
44. Wickham, H.; Seidel, D. *Scales: Scale Functions for Visualization*, R Package Version 1.1.1. 2020. Available online: <https://scales.r-lib.org/> (accessed on 29 June 2022).
45. R Core Team. *A Language and Environment for Statistical Computing*; R Foundation for Statistical Computing: Vienna, Austria, 2021; ISBN 3-900051-07-0.
46. Grünig, B.; Dale, R.; Sjödin, A.; Chapman, B.A.; Rowe, J.; Tomkins-Tinch, C.H.; Valieris, R.; Köster, J. Bioconda: Sustainable and Comprehensive Software Distribution for the Life Sciences. *Nat. Methods* **2018**, *15*, 475–476. [[CrossRef](#)] [[PubMed](#)]
47. Douglas, G.M.; Maffei, V.J.; Zaneveld, J.R.; Yurgel, S.N.; Brown, J.R.; Taylor, C.M.; Huttenhower, C.; Langille, M.G.I. PICRUSt2 for Prediction of Metagenome Functions. *Nat. Biotech.* **2020**, *38*, 685–688. [[CrossRef](#)] [[PubMed](#)]
48. Rösel, A.; Itkin, P.; King, J.; Divine, D.; Wang, C.; Granskog, M.A.; Krumpfen, T.; Gerland, S. Thin Sea Ice, Thick Snow, and Widespread Negative Freeboard Observed During N-ICE2015 North of Svalbard. *J. Geophys. Res. Ocean.* **2018**, *123*, 1156–1176. [[CrossRef](#)]

49. Sun, S.; Jones, R.B.; Fodor, A.A. Inference-Based Accuracy of Metagenome Prediction Tools Varies across Sample Types and Functional Categories. *Microbiome* **2020**, *8*, 46. [[CrossRef](#)]
50. Walker, C.B.; de la Torre, J.R.; Klotz, M.G.; Urakawa, H.; Pinel, N.; Arp, D.J.; Brochier-Armanet, C.; Chain, P.S.G.; Chan, P.P.; Gollabgir, A.; et al. Nitrosopumilus Maritimus Genome Reveals Unique Mechanisms for Nitrification and Autotrophy in Globally Distributed Marine Crenarchaea. *Proc. Natl. Acad. Sci. USA* **2010**, *107*, 8818–8823. [[CrossRef](#)] [[PubMed](#)]
51. Grzymalski, J.J.; Riesenfeld, C.S.; Williams, T.J.; Dussaq, A.M.; Ducklow, H.; Erickson, M.; Cavicchioli, R.; Murray, A.E. A Metagenomic Assessment of Winter and Summer Bacterioplankton from Antarctica Peninsula Coastal Surface Waters. *ISME J.* **2012**, *6*, 1901–1915. [[CrossRef](#)] [[PubMed](#)]
52. Müller, O.; Wilson, B.; Paulsen, M.L.; Rumińska, A.; Armo, H.R.; Bratbak, G.; Øvreås, L. Spatiotemporal Dynamics of Ammonia-Oxidizing Thaumarchaeota in Distinct Arctic Water Masses. *Front. Microbiol.* **2018**, *9*, 24. [[CrossRef](#)] [[PubMed](#)]
53. Luecker, S.; Nowka, B.; Rattei, T.; Spieck, E.; Daims, H. The Genome of Nitrospina Gracilis Illuminates the Metabolism and Evolution of the Major Marine Nitrite Oxidizer. *Front. Microbiol.* **2013**, *4*, 27. [[CrossRef](#)] [[PubMed](#)]
54. Reji, L.; Tolar, B.B.; Smith, J.M.; Chavez, F.P.; Francis, C.A. Differential Co-Occurrence Relationships Shaping Ecotype Diversification within Thaumarchaeota Populations in the Coastal Ocean Water Column. *ISME J.* **2019**, *13*, 1144–1158. [[CrossRef](#)]
55. Wietz, M.; Bienhold, C.; Metfies, K.; Torres-Valdés, S.; von Appen, W.-J.; Salter, I.; Boetius, A. The Polar Night Shift: Seasonal Dynamics and Drivers of Arctic Ocean Microbiomes Revealed by Autonomous Sampling. *ISME Commun.* **2021**, *1*, 76. [[CrossRef](#)]
56. Mori, J.F.; Chen, L.-X.; Jessen, G.L.; Rudderham, S.B.; McBeth, J.M.; Lindsay, M.B.J.; Slater, G.F.; Banfield, J.F.; Warren, L.A. Putative Mixotrophic Nitrifying-Denitrifying Gammaproteobacteria Implicated in Nitrogen Cycling Within the Ammonia/Oxygen Transition Zone of an Oil Sands Pit Lake. *Front. Microbiol.* **2019**, *10*, 2435. [[CrossRef](#)]
57. Liu, Y.; Blain, S.; Crispi, O.; Rembauville, M.; Obernosterer, I. Seasonal Dynamics of Prokaryotes and Their Associations with Diatoms in the Southern Ocean as Revealed by an Autonomous Sampler. *Environ. Microbiol.* **2020**, *22*, 3968–3984. [[CrossRef](#)]
58. Murray, A.E.; Preston, C.M.; Massana, R.; Taylor, L.T.; Blakis, A.; Wu, K.; DeLong, E.F. Seasonal and Spatial Variability of Bacterial and Archaeal Assemblages in the Coastal Waters near Anvers Island, Antarctica. *Appl. Environ. Microbiol.* **1998**, *64*, 2585–2595. [[CrossRef](#)]
59. Mincer, T.J.; Church, M.J.; Taylor, L.T.; Preston, C.; Karl, D.M.; DeLong, E.F. Quantitative Distribution of Presumptive Archaeal and Bacterial Nitrifiers in Monterey Bay and the North Pacific Subtropical Gyre. *Environ. Microbiol.* **2007**, *9*, 1162–1175. [[CrossRef](#)]
60. Smith, J.M.; Chavez, F.P.; Francis, C.A. Ammonium Uptake by Phytoplankton Regulates Nitrification in the Sunlit Ocean. *PLoS ONE* **2014**, *9*, e108173. [[CrossRef](#)]
61. Church, M.J.; DeLong, E.F.; Ducklow, H.W.; Karner, M.B.; Preston, C.M.; Karl, D.M. Abundance and Distribution of Planktonic Archaea and Bacteria in the Waters West of the Antarctic Peninsula. *Limnol. Oceanogr.* **2003**, *48*, 1893–1902. [[CrossRef](#)]
62. Herfort, L.; Schouten, S.; Abbas, B.; Veldhuis, M.J.W.; Coolen, M.J.L.; Wuchter, C.; Boon, J.P.; Herndl, G.J.; Sinninghe Damsté, J.S. Variations in Spatial and Temporal Distribution of Archaea in the North Sea in Relation to Environmental Variables. *FEMS Microbiol. Ecol.* **2007**, *62*, 242–257. [[CrossRef](#)]
63. Morris, R.M.; Rappe, M.S.; Connon, S.A.; Vergin, K.L.; Siebold, W.A.; Carlson, C.A.; Giovannoni, S.J. SAR11 Clade Dominates Ocean Surface Bacterioplankton Communities. *Nature* **2002**, *420*, 806–810. [[CrossRef](#)]
64. West, N.J.; Obernosterer, I.; Zemb, O.; Lebaron, P. Major Differences of Bacterial Diversity and Activity inside and Outside of a Natural Iron-Fertilized Phytoplankton Bloom in the Southern Ocean. *Environ. Microbiol.* **2008**, *10*, 738–756. [[CrossRef](#)] [[PubMed](#)]
65. Schattenhofer, M.; Wulf, J.; Kostadinov, I.; Glöckner, F.O.; Zubkov, M.V.; Fuchs, B.M. Phylogenetic Characterisation of Picoplanktonic Populations with High and Low Nucleic Acid Content in the North Atlantic Ocean. *Syst. Appl. Microbiol.* **2011**, *34*, 470–475. [[CrossRef](#)]
66. Thiele, S.; Fuchs, B.M.; Ramaiah, N.; Amann, R. Microbial Community Response during the Iron Fertilization Experiment LOHAFEX. *Appl. Environ. Microbiol.* **2012**, *78*, 8803–8812. [[CrossRef](#)]
67. Meyer, B.; Kuever, J. Molecular Analysis of the Diversity of Sulfate-Reducing and Sulfur-Oxidizing Prokaryotes in the Environment, Using AprA as Functional Marker Gene. *Appl. Environ. Microbiol.* **2007**, *73*, 7664–7679. [[CrossRef](#)]
68. Thiele, S.; Richter, M.; Balestra, C.; Glöckner, F.O.; Casotti, R. Taxonomic and Functional Diversity of a Coastal Planktonic Bacterial Community in a River-Influenced Marine Area. *Mar. Genom.* **2017**, *32*, 61–69. [[CrossRef](#)]
69. Walsh, D.A.; Zaikova, E.; Howes, C.G.; Song, Y.C.; Wright, J.J.; Tringe, S.G.; Tortell, P.D.; Hallam, S.J. Metagenome of a Versatile Chemolithoautotroph from Expanding Oceanic Dead Zones. *Science* **2009**, *326*, 578–582. [[CrossRef](#)]
70. Sheik, C.S.; Jain, S.; Dick, G.J. Metabolic Flexibility of Enigmatic SAR324 Revealed through Metagenomics and Metatranscriptomics. *Environ. Microbiol.* **2014**, *16*, 304–317. [[CrossRef](#)]
71. Kuever, J.; Rainey, F.A.; Widdel, F. *Desulfuromonas*. In *Bergey's Manual of Systematics of Archaea and Bacteria*; Wiley: Hoboken, NJ, USA, 2015; pp. 1–7. ISBN 978-1-118-96060-8.
72. Simon, M.; Glöckner, F.; Amann, R. Different Community Structure and Temperature Optima of Heterotrophic Picoplankton in Various Regions of the Southern Ocean. *Aquat. Microb. Ecol.* **1999**, *18*, 275–284. [[CrossRef](#)]
73. Puddu, A.; Zoppini, A.; Fazi, S.; Rosati, M.; Amalfitano, S.; Magaletti, E. Bacterial Uptake of DOM Released from P-Limited Phytoplankton. *FEMS Microbiol. Ecol.* **2003**, *46*, 257–268. [[CrossRef](#)]
74. Alderkamp, A.C.; Sintes, E.; Herndl, G.J. Abundance and Activity of Major Groups of Prokaryotic Plankton in the Coastal North Sea during Spring and Summer. *Aquat. Microb. Ecol.* **2006**, *45*, 237–246. [[CrossRef](#)]

75. Gomez-Pereira, P.R.; Fuchs, B.M.; Alonso, C.; Oliver, M.J.; van Beusekom, J.E.E.; Amann, R. Distinct Flavobacterial Communities in Contrasting Water Masses of the North Atlantic Ocean. *ISME J.* **2010**, *4*, 472–487. [[CrossRef](#)]
76. Teeling, H.; Fuchs, B.; Becher, D.; Klockow, C.; Gardebrecht, A.; Bennke, C.M.; Kassabgy, M.; Huang, S.; Mann, A.J.; Waldmann, J.; et al. Substrate-Controlled Succession of Marine Bacterioplankton Populations Induced by a Phytoplankton Bloom. *Science* **2012**, *336*, 608–611. [[CrossRef](#)]
77. Reintjes, G.; Arnosti, C.; Fuchs, B.; Amann, R. Selfish, Sharing and Scavenging Bacteria in the Atlantic Ocean: A Biogeographical Study of Bacterial Substrate Utilisation. *ISME J.* **2019**, *13*, 1119–1132. [[CrossRef](#)]
78. Reintjes, G.; Fuchs, B.M.; Scharfe, M.; Wiltshire, K.H.; Amann, R.; Arnosti, C. Short-Term Changes in Polysaccharide Utilization Mechanisms of Marine Bacterioplankton during a Spring Phytoplankton Bloom. *Environ. Microbiol.* **2020**, *22*, 1884–1900. [[CrossRef](#)]
79. Allers, E.; Gómez-Consarnau, L.; Pinhassi, J.; Gasol, J.M.; Šimek, K.; Pernthaler, J. Response of Alteromonadaceae and Rhodobacteriaceae to Glucose and Phosphorus Manipulation in Marine Mesocosms. *Environ. Microbiol.* **2007**, *9*, 2417–2429. [[CrossRef](#)]
80. Sakami, T.; Watanabe, T.; Kakehi, S.; Taniuchi, Y.; Kuwata, A. Spatial Variation of Bacterial Community Composition at the Expiry of Spring Phytoplankton Bloom in Sendai Bay, Japan. *Gene* **2016**, *576*, 610–617. [[CrossRef](#)]
81. Luria, C.M.; Amaral-Zettler, L.A.; Ducklow, H.W.; Repeta, D.J.; Rhyne, A.L.; Rich, J.J. Seasonal Shifts in Bacterial Community Responses to Phytoplankton-Derived Dissolved Organic Matter in the Western Antarctic Peninsula. *Front. Microbiol.* **2017**, *8*, 2117. [[CrossRef](#)]
82. Mönnich, J.; Tebben, J.; Bergemann, J.; Case, R.; Wohlrab, S.; Harder, T. Niche-Based Assembly of Bacterial Consortia on the Diatom *Thalassiosira rotula* Is Stable and Reproducible. *ISME J.* **2020**, *14*, 1614–1625. [[CrossRef](#)]
83. Park, B.S.; Lee, M.; Shin, K.; Baek, S.H. Response of the Bacterioplankton Composition to Inorganic Nutrient Loading and Phytoplankton in Southern Korean Coastal Waters: A Mesocosm Study. *Mar. Ecol.* **2020**, *41*, e12591. [[CrossRef](#)]
84. Wang, J.; Lu, Y.; Nawaz, M.Z.; Xu, J. Comparative Genomics Reveals Evidence of Genome Reduction and High Extracellular Protein Degradation Potential in *Kangiella*. *Front. Microbiol.* **2018**, *9*, 1224. [[CrossRef](#)] [[PubMed](#)]
85. Thiele, S.; Fuchs, B.M.; Amann, R.; Iversen, M.H. Colonization in the Photic Zone and Subsequent Changes during Sinking Determine Bacterial Community Composition in Marine Snow. *Appl. Environ. Microbiol.* **2015**, *81*, 1463–1471. [[CrossRef](#)] [[PubMed](#)]
86. Xing, P.; Hahnke, R.L.; Unfried, F.; Markert, S.; Huang, S.; Barbeyron, T.; Harder, J.; Becher, D.; Schweder, T.; Glöckner, F.O.; et al. Niches of Two Polysaccharide-Degrading Polaribacter Isolates from the North Sea during a Spring Diatom Bloom. *ISME J.* **2015**, *9*, 1410–1422. [[CrossRef](#)] [[PubMed](#)]
87. Signori, C.N.; Pellizari, V.H.; Enrich-Prast, A.; Sievert, S.M. Spatiotemporal Dynamics of Marine Bacterial and Archaeal Communities in Surface Waters off the Northern Antarctic Peninsula. *Deep Sea Res. II Top. Stud. Oceanogr.* **2018**, *149*, 150–160. [[CrossRef](#)]
88. Liu, Y.; Debeljak, P.; Rembauville, M.; Blain, S.; Obernosterer, I. Diatoms Shape the Biogeography of Heterotrophic Prokaryotes in Early Spring in the Southern Ocean. *Environ. Microbiol.* **2019**, *21*, 1452–1465. [[CrossRef](#)]
89. Martinez-Garcia, M.; Brazel, D.M.; Swan, B.K.; Arnosti, C.; Chain, P.S.G.; Reitenga, K.G.; Xie, G.; Poulton, N.J.; Gomez, M.L.; Masland, D.E.D.; et al. Capturing Single Cell Genomes of Active Polysaccharide Degraders: An Unexpected Contribution of Verrucomicrobia. *PLoS ONE* **2012**, *7*, e35314. [[CrossRef](#)]
90. Cardman, Z.; Arnosti, C.; Durbin, A.; Ziervogel, K.; Cox, C.; Steen, A.D.; Teske, A. Verrucomicrobia Are Candidates for Polysaccharide-Degrading Bacterioplankton in an Arctic Fjord of Svalbard. *Appl. Environ. Microbiol.* **2014**, *80*, 3749–3756. [[CrossRef](#)]
91. Sichert, A.; Corzett, C.H.; Schechter, M.S.; Unfried, F.; Markert, S.; Becher, D.; Fernandez-Guerra, A.; Liebeke, M.; Schweder, T.; Polz, M.F.; et al. Verrucomicrobia Use Hundreds of Enzymes to Digest the Algal Polysaccharide Fucoidan. *Nat. Meth.* **2020**, *5*, 1026–1039. [[CrossRef](#)]
92. Taylor, J.D.; Cottingham, S.D.; Billinge, J.; Cunliffe, M. Seasonal Microbial Community Dynamics Correlate with Phytoplankton-Derived Polysaccharides in Surface Coastal Waters. *ISME J.* **2014**, *8*, 245–248. [[CrossRef](#)]
93. Tisserand, L.; Dadaglio, L.; Intertaglia, L.; Catala, P.; Panagiotopoulos, C.; Obernosterer, I.; Joux, F. Use of Organic Exudates from Two Polar Diatoms by Bacterial Isolates from the Arctic Ocean. *Philos. Trans. R. Soc. A* **2020**, *378*, 20190356. [[CrossRef](#)]